2006-08-21

Optimal Guidance Command Generation and Tracking for Reusable Launch Vehicle Reentry, AIAA (2006; Keystone, Colorado)

AIAA Guidance, Navigation, and Control Conference and Exhibit
21 - 24 August 2006, Keystone, Colorado

AIAA 2006-6691

Optimal Guidance Command Generation and Tracking for Reusable Launch Vehicle Reentry

Kevin P. Bollino*
Naval Postgraduate School, Monterey, CA 93940

Michael W. Oppenheimer† and David D. Doman‡
Air Force Research Laboratory, WPAFB, OH 45433-7531

The objective of this work is to develop a robust guidance and control architecture for autonomous reusable launch vehicles that incorporates elements of recent advances in the areas of optimal trajectory generation and reconfigurable control. This work integrates three separately developed methods to form a coherent architecture with the potential to manage control effector failures, vehicle structural/aerodynamic degradation, uncertainty, and external disturbances. Outer-loop guidance commands in the form of body-frame angular rates (roll, pitch, and yaw) are generated from an optimal reference trajectory that is computed off-line with a direct pseudospectral method and then tracked by a reconfigurable inner-loop control law. The appropriate open-loop state histories from the psuedo-four-degree-of-freedom reference trajectory are converted using a modified backstepping approach that complements the inner-loop control law in a six-degree-of-freedom simulation. The inner-loop control law is capable of reacting and compensating for off-nominal conditions by employing nonlinear reconfigurable control allocation, dynamic inversion, and model-following/anti-windup prefilters. The results show that the inner-loop control can adequately track the desired optimal guidance commands; thus, confirming the applicability of this control architecture for future development involving on-line, optimal trajectory generation and high-fidelity guidance and control for reentry vehicles.

I. Introduction

The safety of manned or unmanned space vehicles returning to earth is of paramount importance. One way to improve their safety is by creating more capable, reliable and efficient guidance, navigation, and control methods. Onboard, real-time optimal trajectory generation, planning, adaptation, reconfiguration, and retargeting are the methods currently being pursued to achieve the autonomous operations needed to facilitate the accomplishment of these objectives.

Previous work by Shaffer [1]-[2] has integrated trajectory reshaping and retargeting with the reconfigurable control work of Oppenheimer et al. [3]-[5], to demonstrate relatively fast computations of optimal trajectories under trim deficient path-constraints. This work used interpolated aerodynamic data that incorporated wing, body and trim effects from a given vehicle flight condition and an optimized effector displacement vector [2]. This essentially decoupled the outer loop from the inner loop. Despite efforts involving on-line approaches [6]-[11], off-line reference trajectories are still used for tracking applications. Since the early days of space shuttle entry guidance, designers have been employing various reference trajectory tracking schemes [12]. Various research has addressed the reentry problem by using an optimal trajectory generator to solve for a reference input trajectory off-line, then use other inner-loop control means to track the desired trajectory [13]-[15]. In some cases, off-line reference

*Ph.D. Candidate, Department of Mechanical and Astronautical Engineering, Guidance, Navigation, and Control Lab, Ph. 831-656-3194, Email: kpbollin@nps.edu, AIAA Member.

†Electronics Engineer, 2210 Eighth Street, Bldg. 146, Rm. 305, Ph. 937-255-8490, Email: Michael.Oppenheimer@wpafb.af.mil, AIAA Member.

‡Senior Aerospace Engineer, 2210 Eighth Street, Bldg. 146, Rm. 305, Ph. 937-255-8451, Email: David.Doman@wpafb.af.mil, AIAA Associate Fellow

trajectories are combined with on-line trajectory generators such as the "Optimum-Path-To-Go" methodology developed by Schierman et al., as previously cited.

In a similar fashion, this paper combines some of the approaches mentioned to demonstrate that a previously developed inner-loop control design, based on dynamic inversion (DI), can successfully track variable body-axis roll, pitch, and yaw commands generated from an off-line, optimal reference trajectory. Note that although the reference trajectory is generated off-line for this paper, concurrent work, as demonstrated in Ref. [16], shows that rapid trajectory generation is capable of providing optimal nonlinear feedback; hence, making this work viable for on-line applications.

To solve the optimal control problem, a spectral algorithm [17]-[19] known as the Legendre Pseudospectral Method is employed by use of a MATLAB-based software package called DIDO [20]. This direct method discretizes the problem and approximates the states, co-states and control variables by use of Lagrange interpolating polynomials where the unknown coefficient values coincide with the Legendre-Gauss-Lobatto (LGL) node points. After this approximation step, a nonlinear program (NLP) solver (SNOPT) solves a sequence of finite-dimensional optimization problems that capture the nonlinearities of the system in the form of an optimal control problem. For an extensive description of this method and its use for reentry applications, see references [1]-[2], [16], and [17]-[22].

The overall goal of this work is to extend recent developments in the areas of optimal trajectory generation and reconfigurable control by forming a robust guidance and control (G&C) architecture that combines three separately developed methods: (1) optimal trajectory generation, (2) guidance command generation based on proportional-integral (PI)-loop closure backstepping, and (3) reconfigurable inner-loop control. The following list identifies the specific objectives for this study.

1. To see how well the inner-loop controller tracks the optimal command histories and remedy any problems
2. To verify what the body-frame angular rates (P,Q,R) should be (steady-state trim values?) since previously assumed constant in other studies
3. To provide initial guesses for other 6-DOF optimal reentry trajectory studies using DIDO
4. To provide a baseline for comparing 6-DOF simulation control deflection histories to optimal deflections computed by a 6-DOF DIDO model
5. To provide a baseline for planned studies involving a single, "integrated" optimal G&C architecture

II. Guidance and Control Design Architecture

The overall G&C design architecture for this work is presented in Fig. 1. The architecture consists of

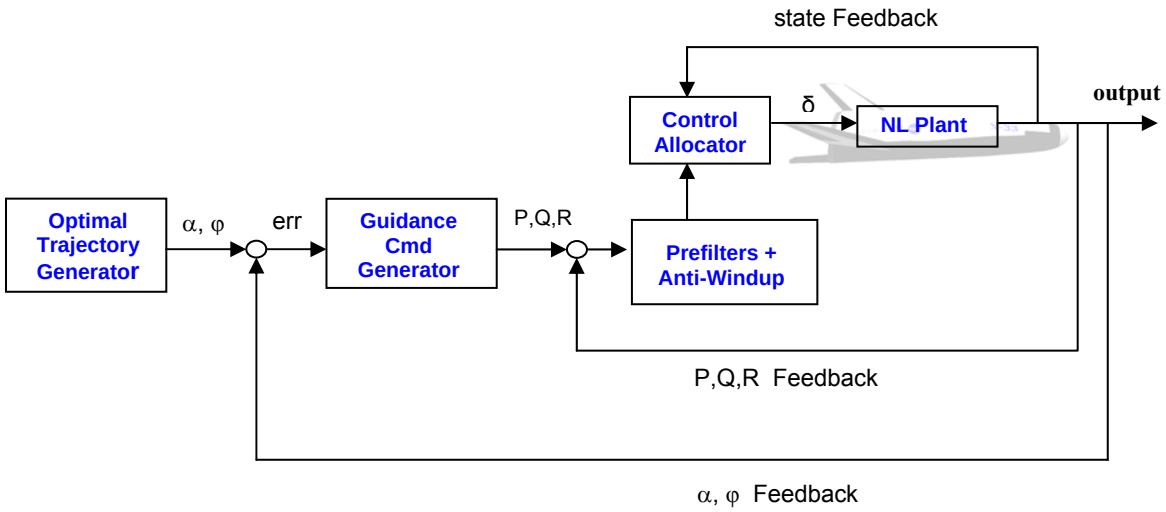

Fig. 1 Conceptual G&C Design Architecture

a two-loop structure: (1) an outer loop that compares the actual angle-of-attack and the bank angle measurements with those provided from the optimal reference trajectory outputs and (2) an inner-loop that is designed to track the

optimal body-rates (P,Q,R) generated from the guidance command generator. For this work, a full, six-degree-of-freedom (6-DOF) model of a reusable launch vehicle (RLV) was employed for the inner-loop tracking simulation whereas the reference trajectory was generated using a psuedo-four-degree-of-freedom (4-DOF) model. Details of the outer and inner-loops are presented in sections III and IV, respectively.

III. Outer-Loop Guidance Command Generation

This section provides some details of how the off-line optimal trajectory is generated with on-line viability and then converted into useful guidance commands.

A. Off-Line, Optimal Trajectory Generation

First, an off-line reference trajectory is generated by posing the reentry problem as a standard optimal control problem (OCP) and solving for the extremal controls using DIDO. For this paper, a reduced-order model is adequate to demonstrate the feasibility of the approach. Thus, the full 6-DOF equations of motion (EoM) are simplified and decoupled. The model used here assumes a point-mass-model over a flat, non-rotating earth such that the positional and translational equations of motion in a Cartesian "local horizontal" coordinate system become

$$\begin{aligned} \dot{x} &= V\cos\gamma\cos\psi \\ \dot{y} &= V\cos\gamma\sin\psi \\ \dot{z} &= V\sin\gamma \\ \dot{V} &= -\frac{D}{m} - g\sin\gamma \\ \dot{\gamma} &= \frac{L}{mV} - \frac{g\cos\gamma}{V} \\ \dot{\psi} &= \frac{L\sin\phi}{mV\cos\gamma} \end{aligned} \tag{1}$$

where x (down-range), y (cross-range), and z (altitude) are the vehicle's position with respect to the fixed-earth reference frame, V is the velocity magnitude (i.e. total equivalent airspeed), γ is the flight-path-angle (FPA), ψ is the heading angle (HA), α is the angle-of-attack (AoA), ϕ is the bank angle (BA), and m is the vehicle's approximate mass during reentry modeled as 2455 slugs (~79,000 lbs). In Eq. (1), the lift and drag forces are represented as L and D, respectively, and are given by

$$L = \frac{1}{2}\rho(z)V^2 C_L(\alpha, M)S_{ref} \tag{2}$$

$$D = \frac{1}{2}\rho(z)V^2 C_D(\alpha, M)S_{ref} \tag{3}$$

where S_{ref} = 1600 ft^2 is the aerodynamic reference area. As noted in Eqs. (2) and (3), the aerodynamic coefficients are assumed to be functions of state variables only:

$$C_L, C_D = f(\alpha, M) \tag{4}$$

and the Mach number and atmospheric density are functions of altitude:

$$M = M(z) \tag{5}$$

$$\rho = \rho(z) \tag{6}$$

The lift and drag coefficients are computed using table lookup data that incorporates wing, body, and trim effects. Likewise, the Mach and density are computed using table lookup data based on a standard 1976 atmospheric model. See Ref. [2] for more details on the use of table lookup data for a similar model.

The optimized controls for this problem are essentially the standard AoA and BA modulation, but to help compensate for command delays (i.e. lags) and to add more realism/fidelity to the problem, as explained in Ref. [1] and [2], the rates of these angles are used as "virtual" controls. This has the benefit of allowing rate limits on AoA and BA which prevents unrealistic responses. Therefore, the control vector is defined as

$$\underline{u} = [u_\alpha,\, u_\phi]^T \in \mathbb{R}^2 \tag{7}$$

and the state vector is

$$\underline{x} = [x\ y\ z\ V\ \gamma\ \psi\ \alpha\ \phi]^T \in \mathbb{R}^8 \tag{8}$$

As with any dynamical optimization problem, the cost function (objective function), governing EoM, path constraints, boundary limits on initial/final conditions, and any constraints (on states and/or controls) must be defined. As such, the general OCP for trajectory generation is fully posed in the following manner:

$$\begin{aligned}
&\min_u\ J\left(\underline{x}(\tau),\underline{u}(\tau),\tau_0,\tau_f\right) = E\left(\underline{x}(\tau_0),\underline{x}(t_f),\tau_0,\tau_f\right) + \int_{\tau_0}^{\tau_f} F\left(\underline{x}(\tau),\underline{u}(\tau),\tau\right) d\tau \\
&\text{subject to} \qquad \dot{\underline{x}} = \underline{f}\left(\underline{x},\underline{u},\tau\right) \\
&\qquad\qquad \underline{h}_l \le \underline{h}\left(\underline{x},\underline{u},\tau\right) \le \underline{h}_u \\
&\qquad\qquad \underline{e}_l \le \underline{e}\left(\underline{x}(\tau_0),\underline{x}(\tau_f),\tau_0,\tau_f\right) \le \underline{e}_u \\
&\qquad\qquad \underline{x}_l \le \underline{x}(\tau) \le \underline{x}_u \\
&\qquad\qquad \underline{u}_l \le \underline{u}(\tau) \le \underline{u}_u
\end{aligned} \tag{9}$$

The goal is to find a state-control function pair, $\{x(\cdot),\, u(\cdot)\}$, or sometimes time, τ, that minimizes the performance index represented by the Bolza form, $J(\cdot)$, consisting of either a Mayer term, $E(\cdot)$, a Lagrange term, $F(\cdot)$, or both as stated above.

Summarizing the previous reentry equations, the specific optimal control formulation for this RLV problem is stated as follows: Given an initial position vector $([x_0,\, y_0,\, z_0])$, velocity magnitude (V_0), FPA (γ_0), heading angle (ψ_0), AoA (α_0), and BA (ϕ_0), find the control history (u_α, u_ϕ) that maximizes the horizontal downrange (x_f) or cross-range (y_f) under various constraints. In the context of Eq. (9) above and for the analysis presented in this work, the cost functions are simply:

$$Min\ \{\ J[\cdot] = -x_f\} \quad -\text{or}- \quad Min\ \{\ J[\cdot] = -y_f\} \tag{10}$$

subject to the dynamic constraints given by Eq. (1), the initial and final event conditions specified as:

$$(t_0, x_0, y_0, z_0, V_0, \gamma_0, \psi_0, \alpha_0, \phi_0) = (0, 0, 0, 125000\,\text{ft}, 5714\frac{\text{ft}}{\text{s}}, -1.3\,\text{deg}, 0, 0\,\text{deg}, 0) \tag{11}$$

$$(z_f, V_f) = (500\,\text{ft}, 335\frac{\text{ft}}{\text{s}}) \tag{12}$$

$$-25\frac{\text{ft}}{\text{s}} \le \dot{z}_f \le 8.33\frac{\text{ft}}{\text{s}} \tag{13}$$

and the state (14), path (15), and control (16) inequality constraints, respectively, specified as

$$\begin{bmatrix} 0 \\ -\infty \\ 0 \\ 0 \\ -90\,\text{deg} \\ -90\,\text{deg} \\ -10\,\text{deg} \\ -90\,\text{deg} \end{bmatrix} \le \begin{bmatrix} x \\ y \\ z \\ V \\ \gamma \\ \psi \\ \alpha \\ \phi \end{bmatrix} \le \begin{bmatrix} \infty \\ \infty \\ \infty \\ \infty \\ 90\,\text{deg} \\ 90\,\text{deg} \\ 50\,\text{deg} \\ 90\,\text{deg} \end{bmatrix} \tag{14}$$

$$\begin{bmatrix} -2.5\text{g's} \\ 0 \\ 0 \end{bmatrix} \le \begin{bmatrix} n_z \\ \bar{q} \\ Q \end{bmatrix} \le \begin{bmatrix} 2.5\text{g's} \\ 600\frac{\text{lb}}{\text{ft}^2} \\ 60\frac{\text{BTU}}{\text{ft-s}} \end{bmatrix} \tag{15}$$

$$-40\frac{\text{deg}}{s} \le u_\alpha, u_\phi \le 40\frac{\text{deg}}{s} \tag{16}$$

where the path constraint terms represent the normal acceleration $n_z = \left| L\cos\alpha + D\sin\alpha \right|$, the dynamic pressure $\bar{q} = \frac{1}{2}\rho(z)V^2$, and the heating rate $Q = k\sqrt{\rho(r)}V^{3.15}$ with constant *k* based on the vehicle's heat shield properties.

B. On-Line, Optimal Trajectory Generation

Although this work computes the optimal reference trajectory off-line and then extracts the appropriate signals to use in the guidance command generation algorithm, preliminary studies conducted concurrently with this work have indicated that the same model using approximated aerodynamic data can solve the problem approximately 85 % faster than using the table look-up data. For example, recent work used a second-order polynomial approximation for lift and drag coefficients and a standard two-parameter exponential atmospheric model that resulted in the successful implementation of a nonlinear sampled-data feedback method with an on-line, trajectory re-optimization scheme that could generate optimal trajectories 99.75 % faster than the same model using the table look-up data [16]. Further work is required to improve the accuracy of the approximations, but initial results look promising for on-line reentry applications.

C. Command Generation via "Backstepping Architecture" (PI & DI)

From the optimal trajectory, the α and ϕ commands are converted into the body-axis angular velocities (P,Q,R) to provide the desired inner-loop commands. The generation of these commands is based on what Schierman defines as a "backstepping" approach whereby the "pseudo-commands" at each loop-closure, using PI-control and DI, drives the next inner-most loop [23]. Common loop closures may consist of an outer-most altitude loop, a FPA loop, and an enclosed inner-most AoA loop.

For this experiment, the 3-DOF DIDO trajectory provides the α and ϕ commands that are then used to generate the body-rate commands (P_{cmd}, Q_{cmd}, R_{cmd}). For example, assuming only longitudinal motion, the appropriate pitch rate command is generated based on the following calculations. Ignoring lateral-directional influences (for now), the wind-axis relation $\alpha = \theta - \gamma$ and the simplified pitch rate $Q = \dot{\theta}$ provide the governing EoM such that

$$\dot{\alpha} = -\dot{\gamma} + Q \tag{17}$$

Also, the governing EoM for the FPA is

$$\dot{\gamma} = \frac{L}{mV} - \frac{g\cos(\theta)}{V} \tag{18}$$

Substituting Eq. (17) into Eq. (18), the resulting pitch-rate command is derived as

$$Q_{cmd} = \dot{\alpha}_{des} + \frac{L}{mV} - \frac{g\cos(\gamma)}{V} \tag{19}$$

To improve α tracking, the desired α dynamics are generated using a proportional feedback controller

$$\dot{\alpha}_{des} = K_{\alpha}(\alpha_{cmd} - \alpha) \tag{20}$$

where α_{cmd} is the optimal α command from the 3-DOF DIDO trajectory. Figure 2 shows a block diagram that represents the computation of the optimal guidance commands.

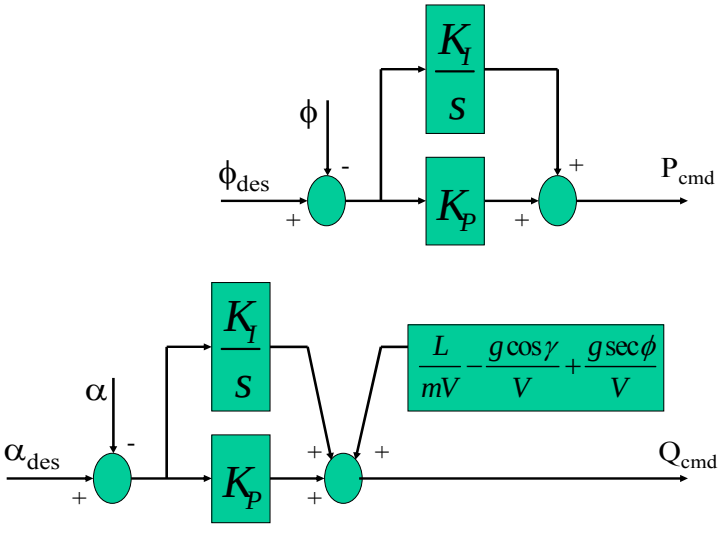

Fig. 2 P and Q Command Generation

Note that for the Q_{cmd} generation in Fig. 2, an extra lateral term is added to account for lateral effects as explained in the results section. Also, not shown in Fig. 2 , is the generation of the yaw command (R_{cmd}) that is computed according to Ref. [27] assuming coordinated turns and is given by

$$R_{cmd} = P_{cmd} \tan\alpha + \frac{g \sin\phi}{u} \tag{21}$$

It is also important to note that throughout this paper the notation ϕ is used for both BA and roll angle since they are assumed equal for this study.

IV. Reconfigurable Inner-Loop Control

This work implemented a 6-DOF simulation containing a reconfigurable inner-loop control algorithm that uses DI, control allocation, and model following prefilters with integrator anti-windup and reference model bandwidth attenuation. Note that although not discussed here for purpose of brevity, the simulation model employs Etkin's standard 6-DOF EoM [28].

A. Dynamic Inversion and Control Allocation

The inner-loop control system uses DI in order to track the desired body-frame angular velocities $(p_{des},\ q_{des},\ r_{des})$. The rotational dynamics for this type of vehicle can be written as:

$$I\dot{\omega} = G_B - \omega \times I\omega \tag{22}$$

where I is the moment-of-inertia tensor, $\omega = [p, q, r]^T$, and G_B is a vector consisting of the total moments acting on the vehicle with contributions from the wing-body-propulsion system (BAE) and the control effectors (δ) such that

$$G_B = G_{BAE}(\omega, P) + G_\delta(P, \delta) = \begin{bmatrix} L \\ M \\ N \end{bmatrix}_{BAE} + \begin{bmatrix} L \\ M \\ N \end{bmatrix}_\delta \tag{23}$$

where L, M, and N are the rolling, pitching, and yawing moments, respectively; the vector P denotes a measurable or estimable quantity that can influence body rates and can contain variables such as AoA, sideslip, Mach number, and mass properties; and δ is a vector of control surface deflections given by $\delta = \left[\delta_1, \delta_2, ..., \delta_n\right]^T$. To design the DI control law, equations (22) and (23) are put into a more standard form by defining $f(\omega, P) \triangleq G_{BAE}(\omega, P) - \omega \times I\omega$ such that

$$I\dot{\omega} = f(\omega, P) + G_\delta(P, \delta) \tag{24}$$

The objective is to find a control law that provides direct control over $\dot{\omega}$ such that $\dot{\omega} = \dot{\omega}_{des}$; therefore, the DI control law must satisfy

$$I\dot{\omega}_{des} - f(\omega, P) = G_\delta(P, \delta) \tag{25}$$

But, since this problem has more control effectors than control variables, a control allocation algorithm is required for a unique solution.

A linear programming based control allocator, which obeys rate and position limits, is used in this work. To implement this type of allocator, the control dependent portion of Eq. (25) must be linear in the controls. Hence, Eq. (25) is rewritten as

$$I\dot{\omega}_{des} - f(\omega, P) = G_{\delta}(P, \delta) = \tilde{G}_{\delta}(P)\delta \tag{26}$$

In order to account for nonlinearities in the moment-deflection relationship, a slope-intercept term is added to Eq. (26) such that

$$I\dot{\omega}_{des} - f(\omega, P) = \tilde{G}_{\delta}(P)\delta + \varepsilon(P, \delta) \tag{27}$$

Then, the final inverse control law becomes

$$\dot{\omega}_{des} - f(\omega, P) - I^{-1}\varepsilon(P, \delta) = I^{-1}\tilde{G}_{\delta}(P)\delta \tag{28}$$

For more details on this DI method and the control allocation algorithm see references [3]-[5] and [23]-[25]. A block diagram representation of the dynamic inversion control law is shown in Fig. 3.

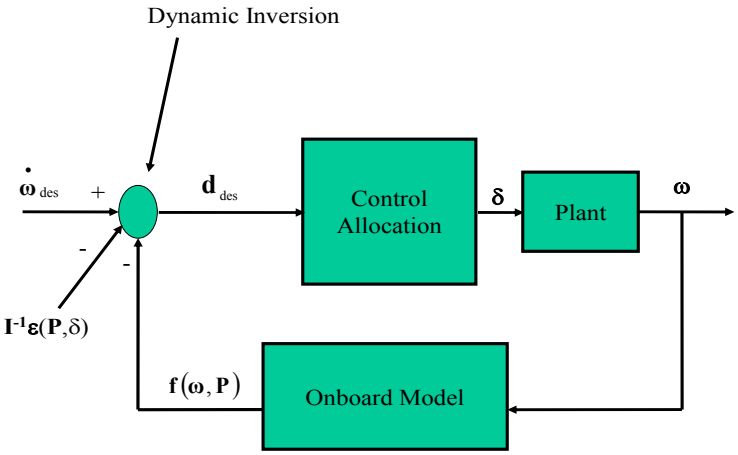

Fig. 3 Dynamic Inversion with Control Allocation

B. Model Following Prefilters

To provide robustness to modeling errors, inversion errors, and to help shape the closed-loop response, prefilters were added to the DI control system as shown in Fig. 4. Previous work involving the inner-loop control designs for the X-40A tested two different prefilter structures: implicit [4] and explicit [23]. For this work, an implicit model-following scheme was selected based on its simplicity in regards to having fewer gains that would ultimately need tuning. Also, it was desired that the closed-inner-loop control system from ω_{des} to ω has the characteristics of a first-order response. The implicit structure presented in Fig. 5 provides this behavior and helps compensate for imperfections in the DI control law. A closer look at this structure with some straight-forward block diagram algebra reveals that a stable pole/zero cancellation occurs. The resulting transfer function displays the desired closed-inner-loop response:

$$\frac{\omega}{\omega_{des}} = \frac{\frac{K_b}{2}}{s + \frac{K_b}{2}} \tag{29}$$

Note that Fig. 5 only displays a single loop; however, the actual model implemented contained a loop for each of the body-axis angular rates.

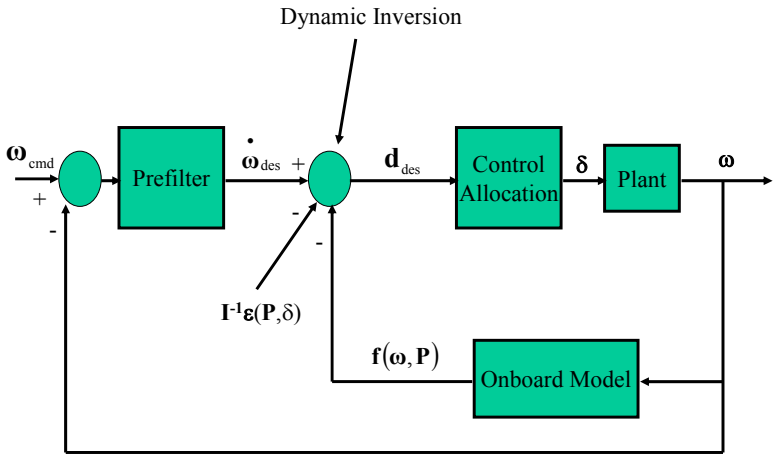

Fig. 4 Dynamic Inversion with Control Allocation and Prefilters

C. Integrator Anti-Windup and Reference Model Bandwidth Attenuation

Axis saturation occurs when all control power is used on one or more axes. For flight control applications, when a control surface moves at its rate limit or resides on a position limit, then control effector saturation occurs. This is a necessary, but not sufficient, situation for axis saturation. With axis saturation, no additional control power is available when requested by the control system and this should be taken into account by the control law. Analysis of the control allocation inputs ($\mathbf{d}_{des}$) and outputs ($\mathbf{B\delta}$) can indicate axis saturation. To prevent canceling tracking errors caused by the axis saturation, the following integrator anti-windup law is added to reduce the magnitude of input signal to the integrator.

$$I_{AW} = K_{AW}(B\delta_{cmd} - d_{des}) \tag{30}$$

where K_{AW} is the anti-windup gain, d_{des} is the desired accelerations from the control effectors, and $B\delta_{cmd}$ is what the control allocator thinks is being produced by the effectors. If no saturation occurs, then $B\delta_{cmd} - d_{des} = 0$ and the control law operates normally; otherwise, at least one axis is saturated and the state of the prefilter integrator is reduced by the anti-windup signal. The anti-windup scheme is implemented as depicted in Fig. 5.

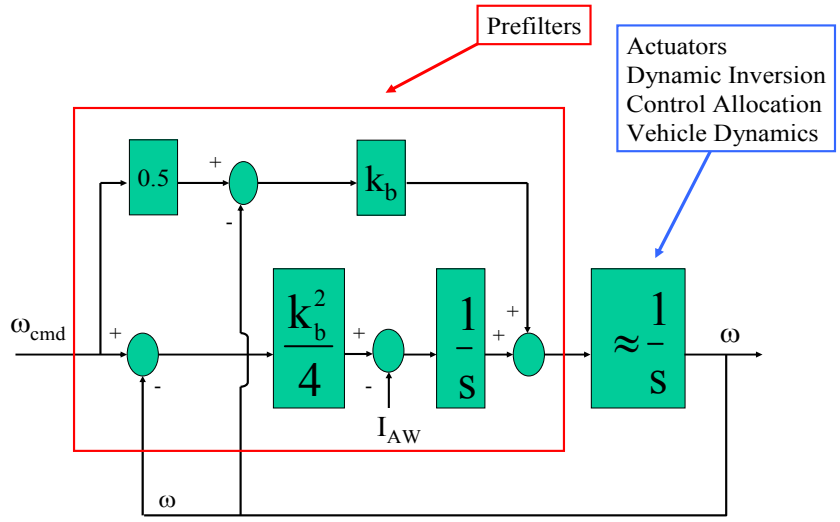

Fig. 5 Implicit Model Following Prefilter Integrator Anti-Windup Compensation

For more details on the anti-windup integrator and its use see Ref. [26] and [23].

V. Results and Discussions

The primary performance concerns for this work were tracking error and control saturation. Of course the overall index of performance is that the cost functions for both the outer-loop guidance and inner-loop control agree to within an acceptable tolerance. As long as the desired trajectory and cost were accomplished, the tracking performance was only graphically confirmed. For this paper, only the max downrange and max cross-range results are presented.

A. Max Downrange (DR) Case

For the case of maximizing the vehicle's downrange distance, the 3-DOF optimal trajectory is generated off-line and α and ϕ histories are extracted for use as the desired guidance commands. These command profiles are shown in Fig. 6.

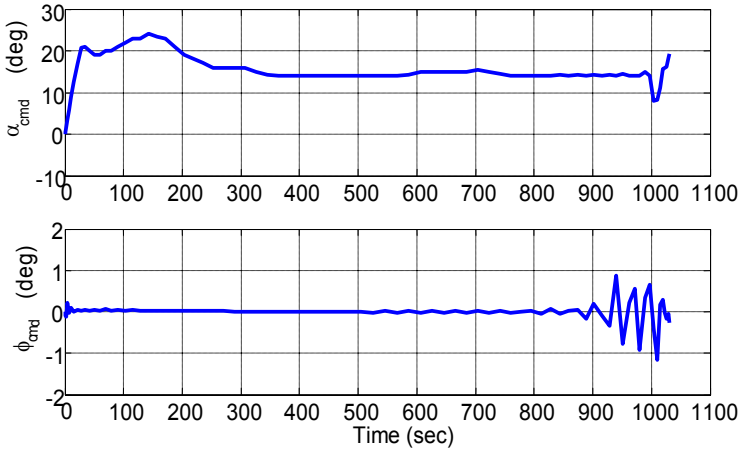

Fig. 6 Max DR Commands from 3-DOF Optimal Reference Trajectory

Initial comparison of the PQR-guidance commands with the actual PQR-states revealed that the inner-loop controller was successfully tracking the desired values; however, when comparing the actual states to those of the reference trajectory, there were some unacceptable errors, especially for α. After carefully reviewing the data, trial-and-error gain tuning on the prefilter and anti-windup gains, it was determined that adding an integrator in the command generation block, Fig. 2, improves the reference trajectory tracking as shown in Fig. 7. With this

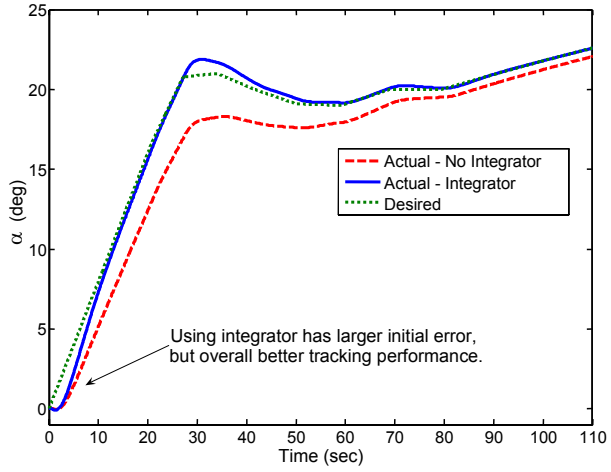

Fig. 7 Comparison of AoA with and without Integrator in Command Generation Logic

addition and use of the gains in Table 1, the max DR results were acceptable with an average difference of only 2 % between the actual and commanded/desired values as seen in figures 9, 10, and 11. The cost for the optimal reference trajectory and the simulation were 1,515,588 ft and 1,515,852 ft, respectively, which results in only a 0.017 % error.

Table 1 Tuned Gains used in Inner-Loop Control System

Gain Type	Max DR	Max CR
Prefilter BW, P (K_{bP})	5.0	4.0
Prefilter BW, Q (K_{bQ})	5.0	4.0
Prefilter BW, R (K_{bR})	5.0	4.0
Proportional DI (K_P)	0.8	0.9
Integral DI (K_I)	0.5	0.5
Anti-Windup, P ($K_{AW,P}$)	0.2	0.1
Anti-Windup, Q ($K_{AW,Q}$)	0.2	0.1
Anti-Windup, R ($K_{AW,R}$)	0.2	0.1

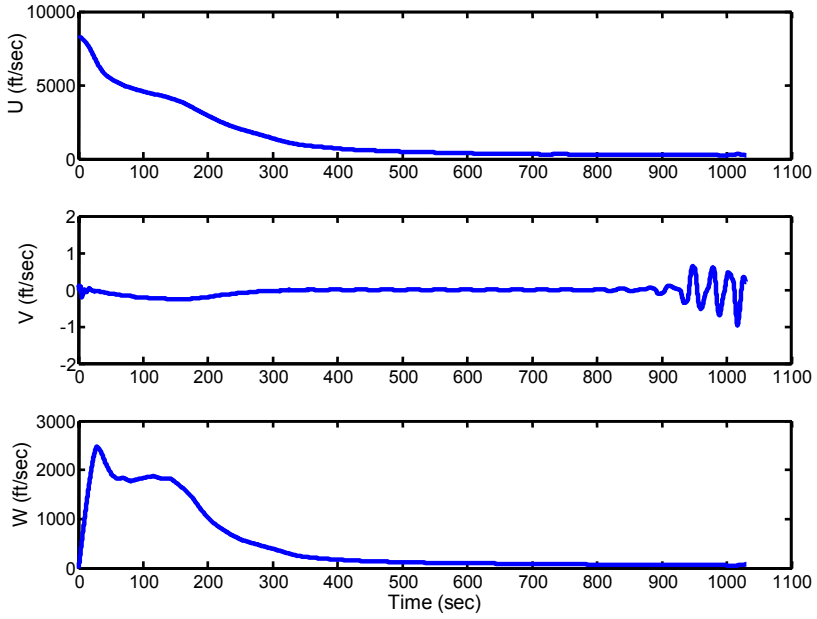

Fig. 8 Max DR Linear Velocities (U,V,W)

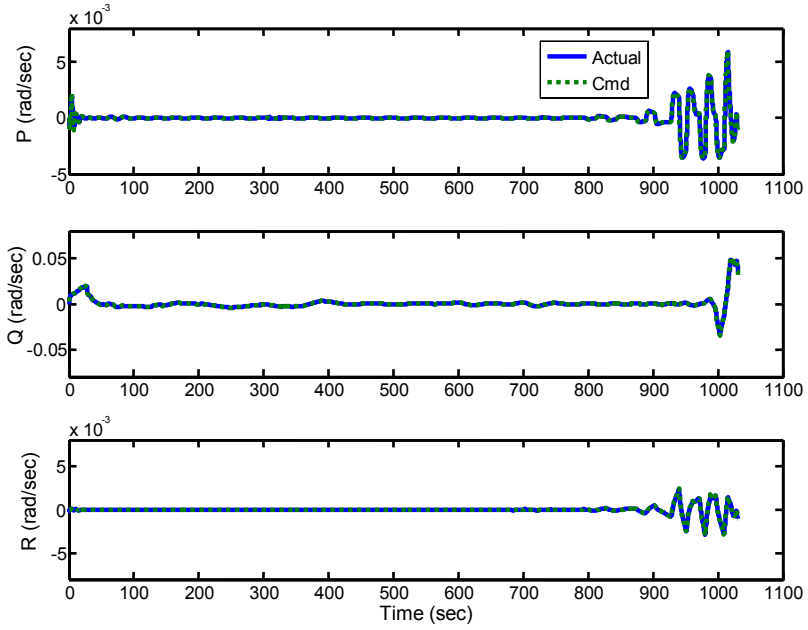

Fig. 9 Max DR Angular Body-Rates (P,Q,R)

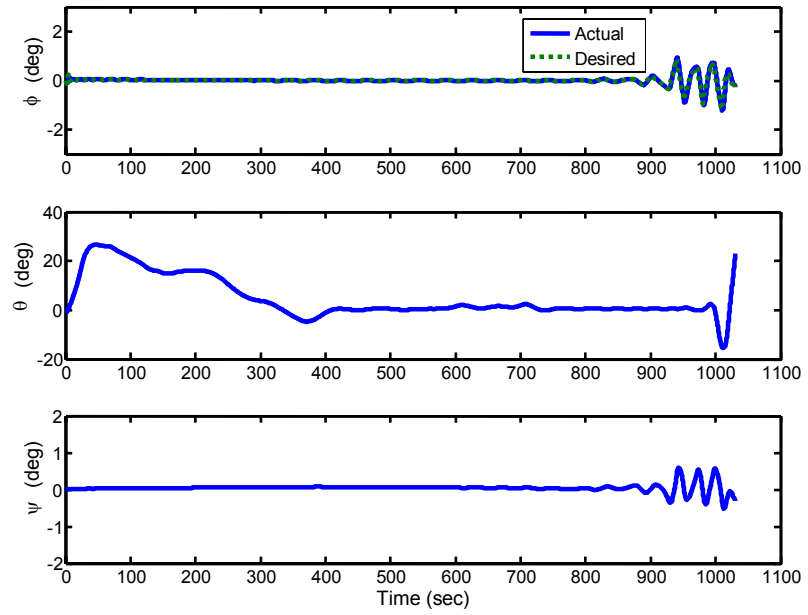

Fig. 10 Max DR Euler Angles (Phi, Theta, Psi)

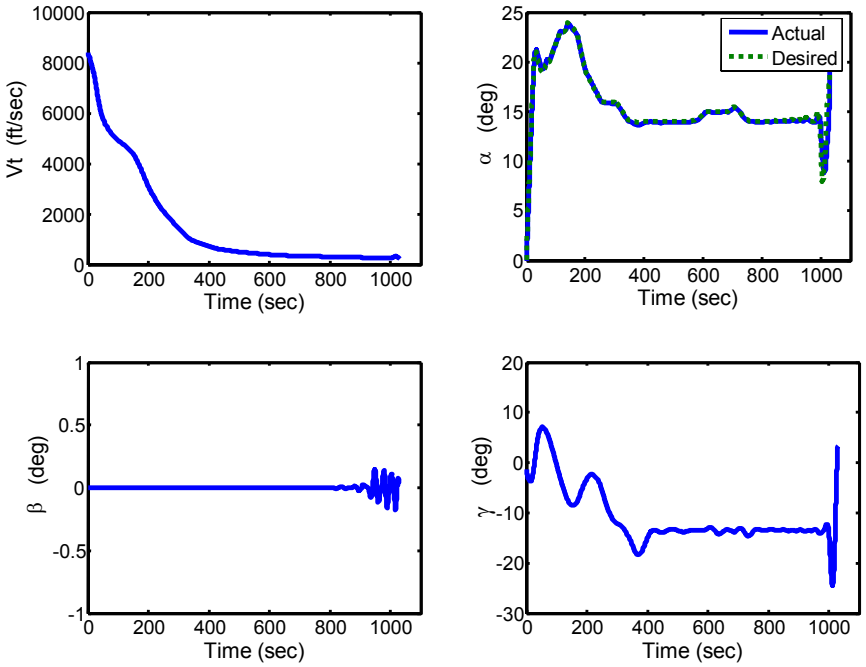

Fig. 11 Max DR Airspeed (V) and Wind-Relative Angles (Alpha, Beta, Gamma)

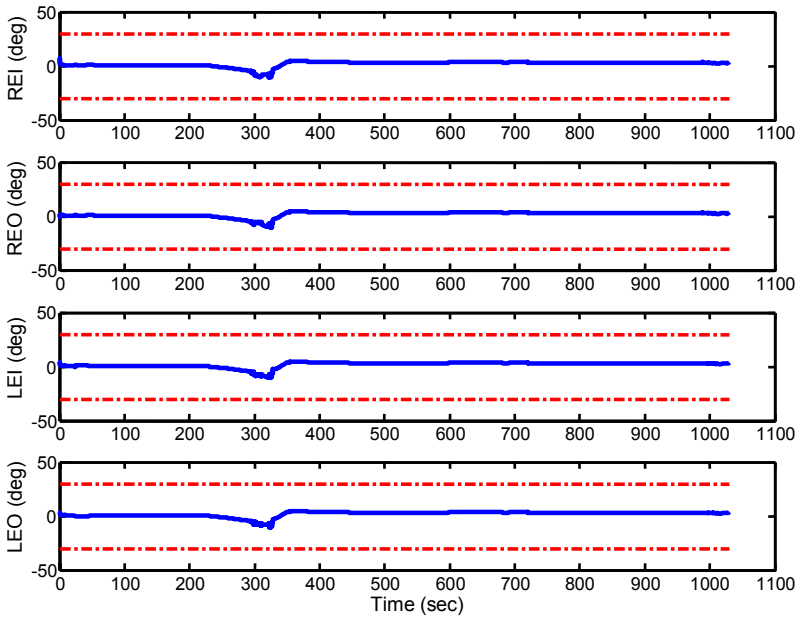

Fig. 12 Max DR Elevon Control Surface Deflections (Right Elevon Inboard, etc…)

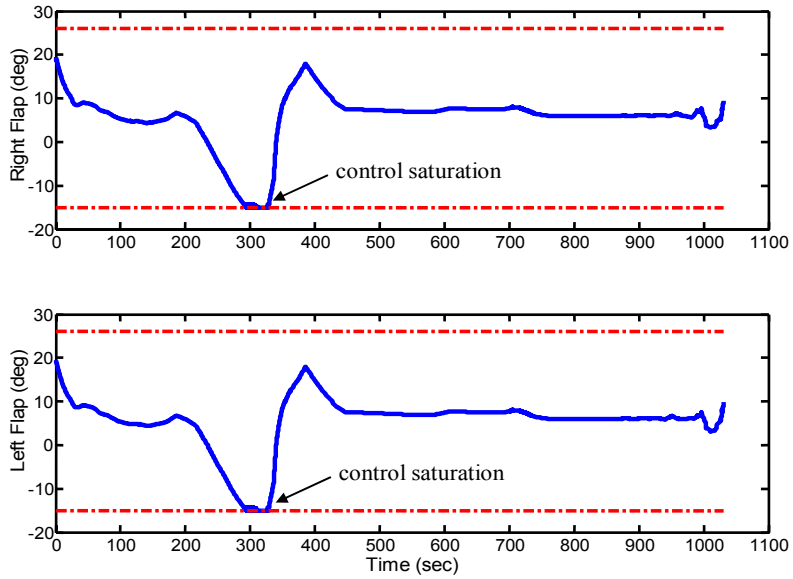

Fig. 13 Max DR Body Flap Control Surface Deflections

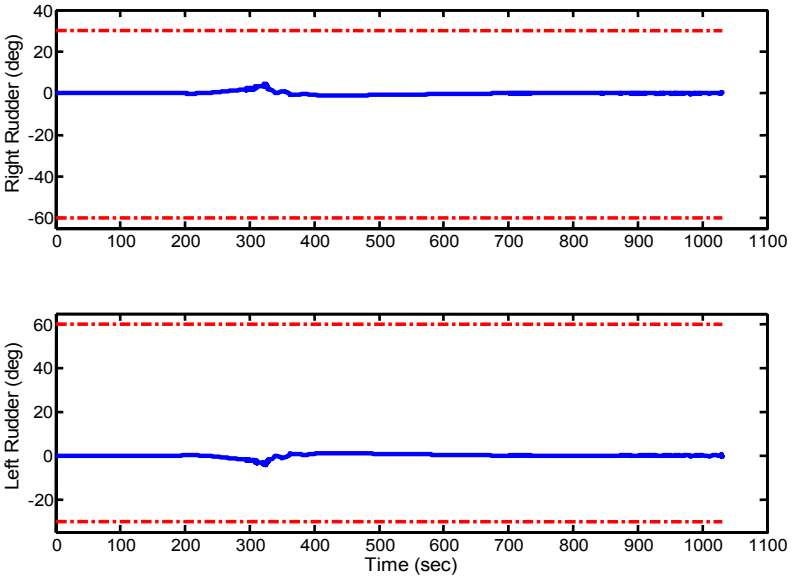

Fig. 14 Max DR Rudder Control Surface Deflections

Figures 12-14 show that all of the control surface deflections in the 6-DOF simulation remain within their respective limits as indicated by the dash-dot lines. As indicated in Fig. 13, there is only one region of body-flap control saturation from approximately 290-325 sec that may be related to an initial pitch down attitude just prior to what appears to be a steady-state trimmed condition from approximately 425-980 sec. Figure 15 shows that the anti-windup values remain approximately zero (10^{-15}) throughout the flight simulation.

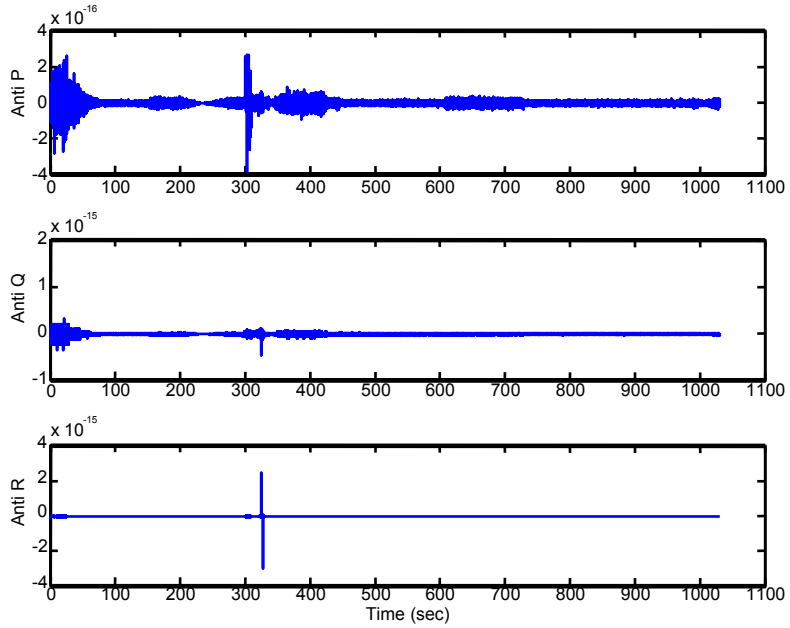

Fig. 15 Max DR Anti-Windup Signals

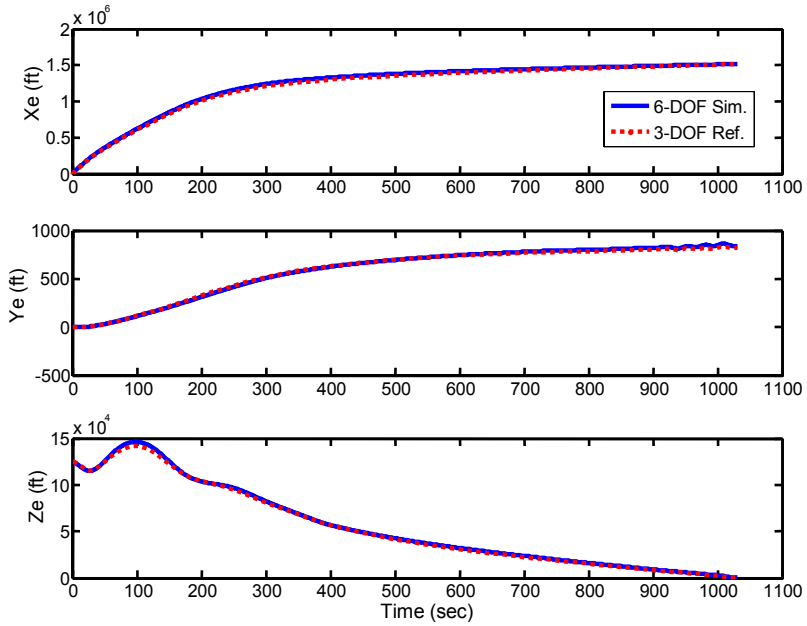

Fig. 16 Max DR Comparison of Reference and Tracking Trajectory

In addition to checking that the system adequately tracks the desired guidance commands, Fig. 16 shows that these commands result in an acceptable reentry trajectory when comparing the 6-DOF simulation and the 3-DOF reference x,y,z-state histories.

B. Max Cross-Range (CR) Case

For the case of maximizing the vehicle's cross-range distance, α and ϕ histories are extracted from the off-line optimal trajectory as was done for the max DR case. These command profiles are shown in Fig. 18.

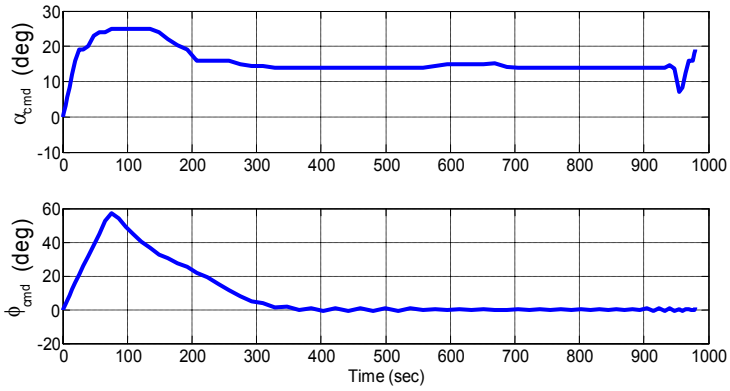

Fig. 17 Max CR Commands from 3-DOF Optimal Reference Trajectory

For maneuvers with large bank angles, such as the max CR case, there is a loss of lift that must be countered in order to maintain altitude. Typically, the elevator is used to provide more lift. In short, the longitudinal and lateral equations of motion are strongly coupled during maneuvers with large bank angles. For example, a pilot must maintain adequate backpressure on the yoke during steep turns to prevent loss of altitude. To account for this in the pitch-command (Q_{cmd}) generation, the following extra lift term [28] was added to provide the appropriate contribution from the bank angle:

$$L = mg\sec(\phi) \Rightarrow \frac{g}{V}\sec(\phi) \tag{31}$$

Similarly, the simplifying assumption that $\dot{\theta} = Q$ used for the backstepping architecture in section III.C is only valid when the roll angle (ϕ) is sufficiently small. For the maximum CR trajectory where the roll angle may be large, it is better to use the relation $\dot{\theta} = Q\cos\phi - R\sin\phi$ [28] such that Eq. (17) becomes

$$\dot{\alpha} = -\dot{\gamma} + Q\cos\phi - R\sin\phi \tag{32}$$

and Eq. (19) becomes

$$Q_{cmd} = \left[\dot{\alpha}_{des} + \frac{L}{mV} - \frac{g\cos(\gamma)}{V} + R\sin\phi\right]\sec\phi \tag{33}$$

Of course, this still has the implied assumption that $\alpha = \theta - \gamma$ which in only valid for "wings-level" flight, but including Eq. (31) helps compensate for this.

With this addition and use of the gains in Table 1, the max CR results were acceptable with only an average difference of 2.2 % between the actual and commanded/desired values as seen in figures 19, 20, and 21. The cost for the optimal reference trajectory and the simulation were 664,862 ft and 671,781ft, respectively, which results in only a 1.04 % error.

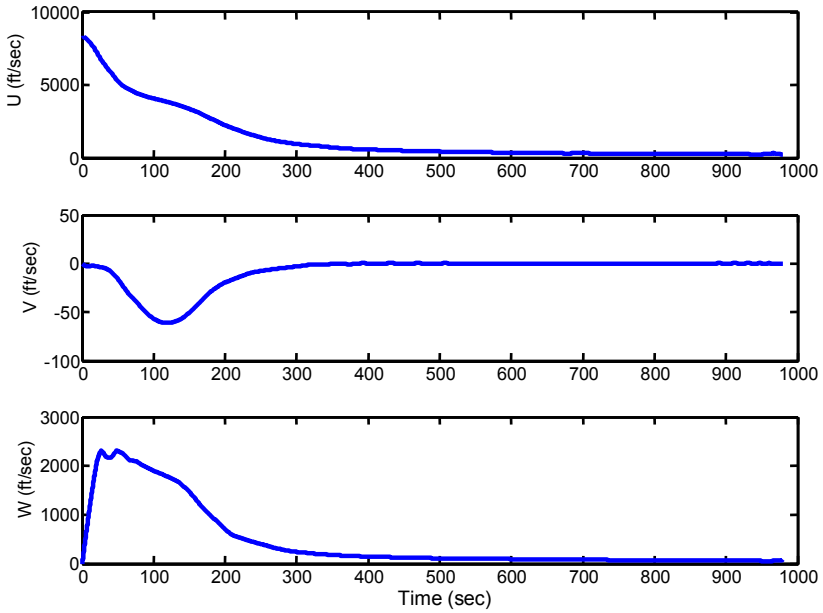

Fig. 18 Max CR Linear Body-Relative Velocities (U,V,W)

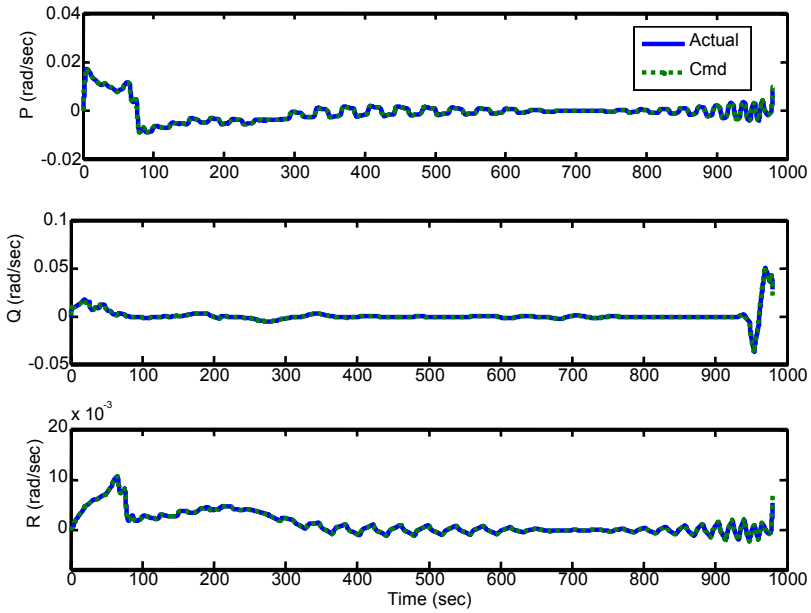

Fig. 19 Max CR Angular Body-Rates (P,Q,R)

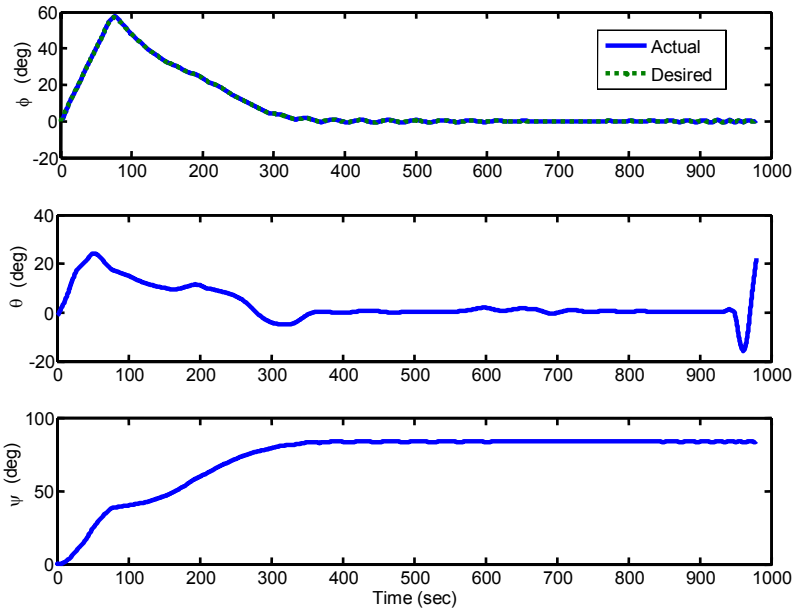

Fig. 20 Max CR Euler Angles (Phi, Theta, Psi)

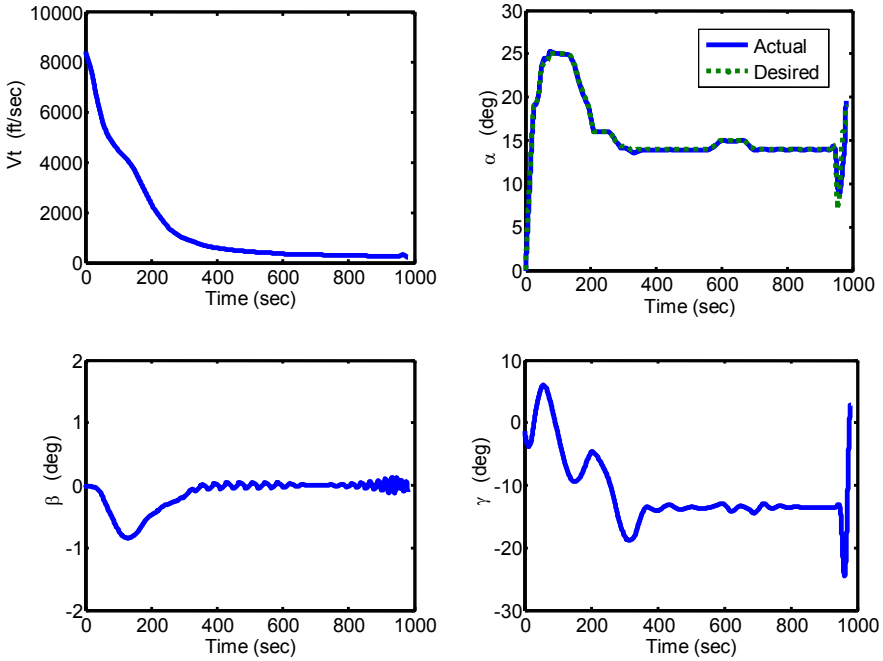

Fig. 21 Max CR Airspeed (V) and Wind-Relative Angles (Alpha, Beta, Gamma)

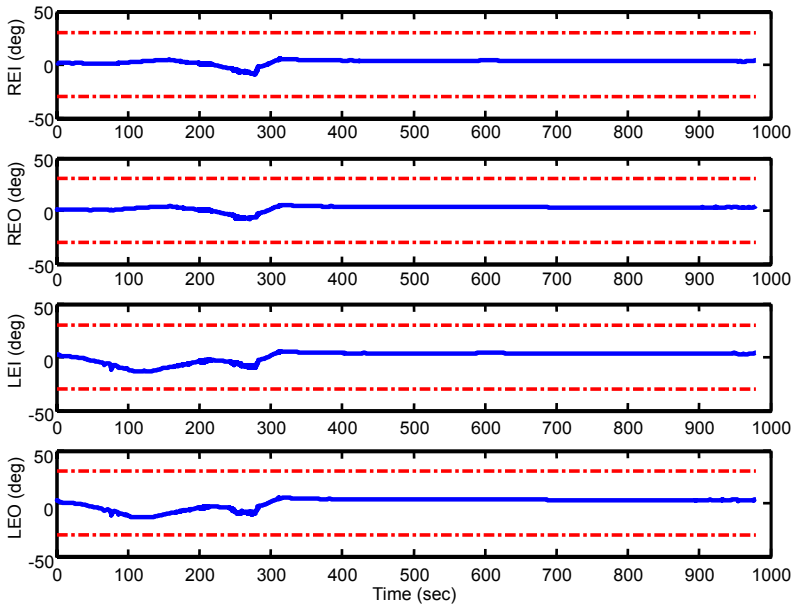

Fig. 22 Max CR Elevon Control Surface Deflections

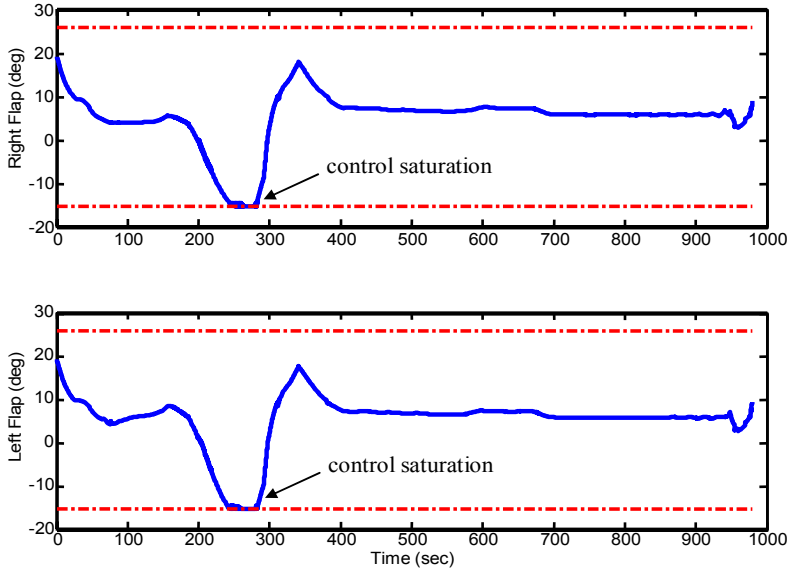

Fig. 23 Max CR Body Flap Control Surface Deflections

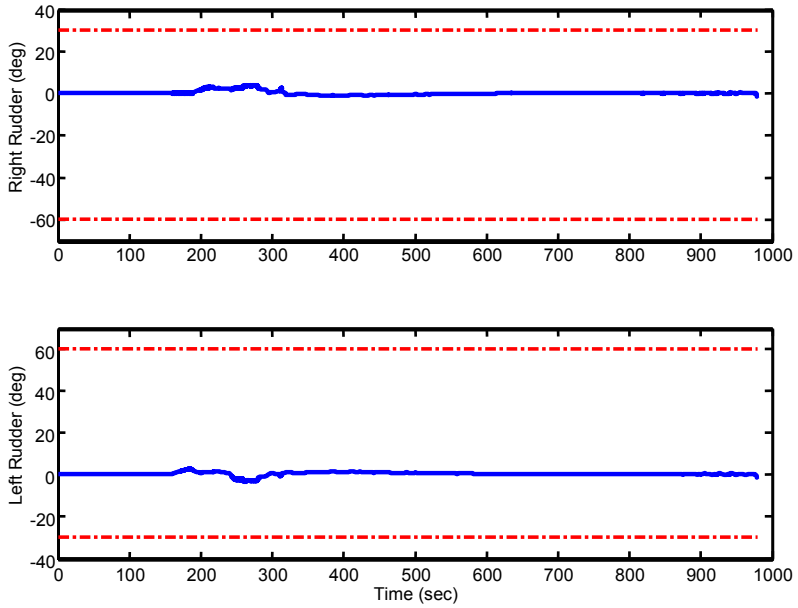

Fig. 24 Max CR Rudder Control Surface Deflections

Similar to the max DR case, Figures 22-24 show that all of the control surface deflections in the 6-DOF simulation remain within their respective limits as indicated by the dash-dot lines. Again, as indicated in Fig. 23, there is only one region of body-flap control saturation from approximately 240-280 sec. Also, Fig. 25 shows that the anti-windup values remain approximately zero (10^{-15}) throughout the flight simulation.

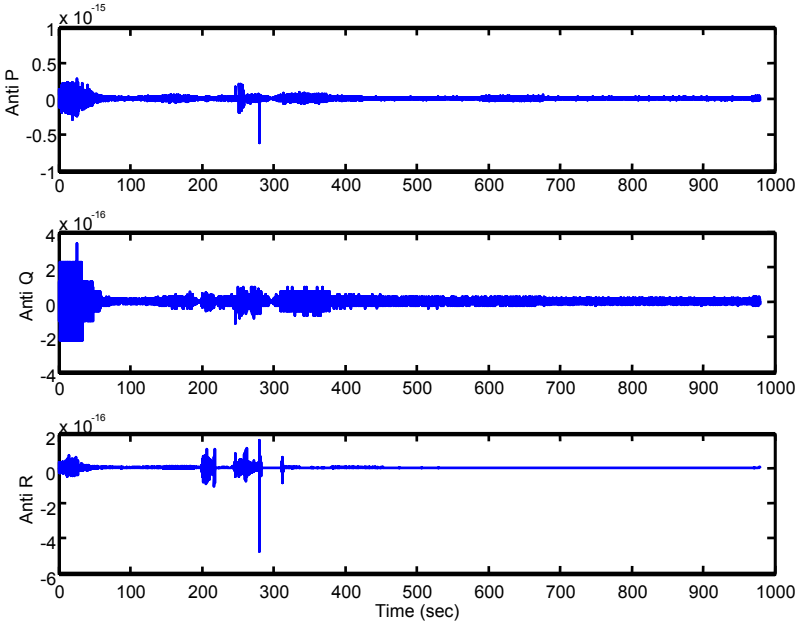

Fig. 25 Max CR Anti-Windup Signals

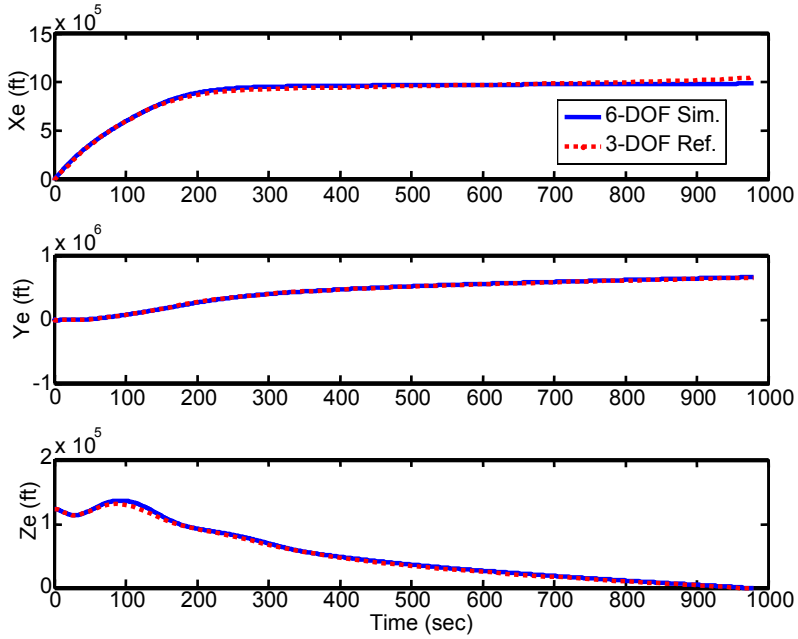

Fig. 26 Max CR Comparison of Reference and Tracking Trajectory

Figure 26 verifies that the guidance commands result in an acceptable reentry trajectory when comparing the 6-DOF simulation and the 3-DOF reference x,y,z-state histories.

VI. Conclusions

This paper presented the successful integration of a reconfigurable inner-loop control law consisting of DI, control allocation, model reference prefilters, and anti-windup integrators with an outer-loop, optimal guidance command generator. As demonstrated, the inner-loop control law was capable of tracking the body-frame angular rates that were converted from the wind-relative α and ϕ modulation of the off-line reference trajectory. Although the optimal trajectory generation was done off-line for this work, a similar model has already been demonstrated to work for on-line reentry applications using the same direct Legendre pseudospectral method [16].

The potential drawback of the presented G&C architecture is that the inner-loop control system depends on various gains that require off-line tuning. This may limit the system's use for on-board autonomous applications, especially in situations involving unplanned maneuvers and/or flight anomalies. Even with the added robustness provided by the prefilters, anti-windup mechanism, and the reconfigurable control, additional modifications may still be needed to handle unexpected operational conditions. With this said, concurrent and future work involves the development of fully autonomous systems that can account for any unforeseen circumstances, including, but not limited to uncertain aerodynamics, significant external disturbances, control failures, and vehicle damage.

Acknowledgments

This work was sponsored by the Air Force Research Laboratory (AFRL/VACA), WPAFB, Ohio, with assistance provided by Dr. David Doman, the Technical Area Leader for the Space Access and Hypersonic Vehicle Guidance and Control Group. His 'guidance' on this work is greatly appreciated.

References

1. Shaffer, P.J., Ross, I.M., Oppenheimer, M.W., Doman, D.B., "Optimal Trajectory Reconfiguration and Retargeting for a Reusable Launch Vehicle," *Proceedings of the 2005 AIAA Guidance, Navigation, and Control Conference*, AIAA Paper No. 2005-4168, Aug 2005.
2. Shaffer, Patrick J., *Optimal Trajectory Reconfiguration and Retargeting for the X-33 Reusable Launch Vehicle*, Thesis, Naval Postgraduate School, Monterey, CA, 2004.
3. Oppenheimer, M.W., and Doman, D.B., "Reconfigurable Control Design for the X-40A with In-Flight Simulation Results," *Proceedings of the 2005 AIAA Guidance, Navigation, and Control Conference*, AIAA Paper No. 2004-5017, Aug 2004.
4. Oppenheimer, M.W., and Doman, D.B., "Reconfigurable Inner Loop Control of a Space Maneuvering Vehicle," *Proceedings of the 2003 AIAA Guidance, Navigation, and Control Conference*, AIAA Paper No. 2003-5358, Aug 2003.
5. Doman, D.B., and Oppenheimer, M.W., "Integrated Adaptive Guidance and Control for Space Access Vehicles, Volume 1: Reconfigurable Control Law for X-40A Approach and Landing," *AFRL IAG&C Technical Report*, Wright-Patterson AFB, OH, 2004.
6. Pesch, H.J., "Off-Line and On-Line Computation of Optimal Trajectories in the Aerospace Field," Prepared for the 12th Course in *Applied Mathematics in the Aerospace Field* of the International School of Mathematics, Ettore Majorana Centre for Scientific Culture, Sicily, Sept 1991.
7. Shen, Z. and Lu, P., "Onboard Generation of Three-Dimensional Constrained Entry Trajectories," *Journal of Guidance, Control, and Dynamics*, Vol. 26, No. 1, pp.111-121, 2003.
8. Allwine, D.A., Fisher, J.E., Strahler, J.A., Lawrence, D.A., Oppenheimer, M.W., and Doman, D.B., "On-Line Trajectory Generation for Hypersonic Vehicles," *Proceedings of the 2005 AIAA Guidance, Navigation, and Control Conference*, AIAA Paper No. 2005-6435, Aug 2005.
9. Verma, A., Oppenheimer, M.W., and Doman, D.B., "On-Line Adaptive Estimation and Trajectory Reshaping," *Proceedings of the 2005 AIAA Guidance, Navigation, and Control Conference*, AIAA Paper No. 2005-6436, Aug 2005.
10. Schierman, J.D., Hull, J.R., and Ward, D.G., "On-Line Trajectory Command Reshaping for Reusable Launch Vehicles," *Proceedings of the 2003 AIAA Guidance, Navigation, and Control Conference*, AIAA Paper No. 2003-5439, Aug 2003.
11. Schierman, J.D., Hull, J.R., "In-Flight Entry Trajectory Optimization for Reusable Launch Vehicles," *Proceedings of the 2005 AIAA Guidance, Navigation, and Control Conference*, AIAA Paper No. 2005-6434, Aug 2005.
12. Harpold, J C., and Graves, C.A., "Shuttle Entry Guidance," *The Journal of Astronuatical Sciences*, Vol. 27, No. 3, pp.239-268, Jul-Sep 1979.
13. Schierman, J.D., Ward, D.G., Monaco, J.F., and Hull, J.R., "Reconfigurable Guidance Approach for Reusable Launch Vehicles," *Proceedings of the 2001 AIAA Guidance, Navigation, and Control Conference*, AIAA Paper No. 2001-4429, Aug 2001.
14. Schierman, J.D., Hull, J.R., and Ward, D.G., "Adaptive Guidance with Trajectory Reshaping for Reusable Launch Vehicles," *Proceedings of the 2002 AIAA Guidance, Navigation, and Control Conference*, AIAA Paper No. 2002-4458, Aug 2002.
15. Carson, J.M., Epstein, M.S., MacMynowski, D.G., and Murray, R.M., "Optimal Nonlinear Guidance with Inner-Loop Feedback for Hypersonic Re-Entry," *Proceedings of the 2006 American Control Conference*, IEEE Paper, Jun 2006.
16. Bollino, K.P., Ross, I.M., and Doman, D.B., "Optimal Nonlinear Feedback Guidance for Reentry Vehicles," *Proceedings of the 2006 AIAA Guidance, Navigation, and Control Conference*, AIAA Paper No. 2006-6074, Aug 2006.
17. Ross, I.M., and Fahroo, F., "Legendre Pseudospectral Approximations of Optimal Control Problems," *Lecture Notes in Control and Information Sciences*, Vol. 295, Springer-Verlag, new York, pp.327-342, 2003.
18. Ross, I.M., and Fahroo, F., "Pseudospectral Knotting Methods for Solving Optimal Control Problems," *Journal of Guidance, Control, and Dynamics*, Vol. 27, No. 3, pp.397-405, 2004.

19. Ross, I.M., Fahroo, F., and Gong, Q., "A Spectral Algorithm for Pseudospectral Methods in Optimal Control," *Proceedings of the 6th IASTED International Conference on Intelligent Systems and Control*, Honolulu, HI, 2004.
20. Ross, I.M., and Fahroo, F., "User's Manual for DIDO 2002: A MATLAB Application Package for Dynamic Optimization," NPS Technical Report AA-02-002, Department of Aeronautics and Astronautics, Naval Postgraduate School, Monterey, CA, June 2002.
21. Josselyn, S. and Ross, I.M., "Rapid Verification Method for the Trajectory Optimization of Reentry Vehicles," *Journal of Guidance, Control, and Dynamics*, Vol.26, No. 3, pp.505-508, 2002.
22. Fahroo, F., and Doman, D., "A Direct Method for Approach and Landing Trajectory Reshaping with Failure Effect Estimation," *Proceedings of the 2004 AIAA Guidance, Navigation, and Control Conference*, AIAA Paper No. 2004-4772, Aug 2004.
23. Schierman, J.D., Hull, J.R., Gandhi, N., and Ward, D.G., "Flight Test Results of an Adaptive Guidance System for Reusable Launch Vehicles," *Proceedings of the 2004 AIAA Guidance, Navigation, and Control Conference*, AIAA Paper No. 2004-4771, Aug 2004.
24. Bolender, M.A., and Doman, D.B., Nonlinear Control Allocation Using Piecewise Linear Functions," *Journal of Guidance, Control, and Dynamics*, Vol.27, No. 6, pp.1017-1027, 2004.
25. Doman, D.B., and Oppenheimer, M.W., "Improving Control Allocation Accuracy for Nonlinear Aircraft Dynamics," *Proceedings of the 2002 AIAA Guidance, Navigation, and Control Conference*, AIAA Paper No. 2005-4667, Aug 2002.
26. Oppenheimer, M.W., and Doman, D.B., "Methods for Compensating for Control Allocator and Actuator Interactions," *Proceedings of the 2004 AIAA Guidance, Navigation, and Control Conference*, AIAA Paper No. 2004-5168, Aug 2004.
27. McLean, Donald, *Automatic Flight Control Systems*, Prentice Hall, Cambridge, 1990.
28. Etkin, Bernard, *Dynamics of Atmospheric Flight*, John Wiley & Sons, New York, 1972.